This is the accepted manuscript version of:
Wang C, Tremblay R, Rogers CA (2021) "Parametric study on the I-shape brace connection of conventional concentrically braced frames", Journal of Constructional Steel Research 182: 106669. doi: /10.1016/j.jcsr.2021.106669

Parametric Study on the I-shape Brace Connection of Conventional Concentrically Braced Frames

Chen Wang[1], Robert Tremblay[2], Colin A. Rogers[3]

[1] Graduate Research Assistant, Department of Civil Engineering, McGill University, Montreal, QC, Canada.
Email: chen.wang5@mail.mcgill.ca

[2] Professor, Department of Civil, Geological and Mining Engineering, Polytechnique Montréal, Montreal, QC, Canada.
Email: robert.tremblay@polymtl.ca

[3] Corresponding author
Professor, Department of Civil Engineering, McGill University, Montreal, QC, Canada.
Email: colin.rogers@mcgill.ca
817 Sherbrooke Street West
Montreal, QC, Canada, H3A 0C3
Tel. 514 398-6449

Abstract

Concentrically braced frames (CBFs), designed using the conventional linear elastic method without seismic proportioning and detailing requirements, are referred to as Conventional CBFs (CCBFs) in this study. They are widely used in moderate and low seismic areas in North America due to the ease of design and economy. Without a code specified dedicated fuse member to dissipate earthquake induced energy, or a prescribed yield/failure hierarchy, the brace connection of a CCBF is usually the weakest link in the lateral load-carrying path and prone to fracture. The brace connection is therefore determinant for the structural seismic performance. In this paper, a parametric study based on a validated numerical simulation procedure was carried out on a typical I-shape brace connection, i.e. the flange plate connection. Three key design parameters, namely, the gusset plate thickness, the flange lap plate thickness, and the web lap plate thickness, were varied to study their effects on both the compressive and tensile behaviour of the brace and connection assembly. Various possible failure modes were revealed both in compression and in tension. The results showed that the brace end restraint provided by flange plate connections in CCBFs was significant; the pinned-end assumption would lead to conservative estimation of the brace buckling resistance, which might trigger detrimental gusset plate buckling. The tensile overstrength of the flange lap plate, due to the presence of transverse tensile stress along the net section, was quantified using the von Mises criterion. Design recommendations are proposed with regards to attaining better deformation capacity.

Keywords: conventional CBFs, I-shape brace, flange plate connection, FE simulation, parametric study

1. Introduction

The choice of concentrically braced frames (CBFs) as the seismic force resisting system (SFRS) of steel buildings is prevalent in North America owing to their efficiency and economy in providing the required lateral strength and stiffness. In areas of high seismic hazard, the capacity design principle along with rigorous detailing and proportioning rules are generally required for the design of CBFs, e.g. the Special Concentrically Braced Frames (SCBFs) in the ASCE/SEI 7-16 [1] and the Moderately Ductile (Type MD) CBFs in the National Building Code of Canada (NBCC) [2]. The plastic behaviour in these systems is restricted to the bracing members, while all the other framing members and connections in the lateral load path are designed to remain essentially elastic when subjected to severe earthquake shaking [3].

However, in moderate or low seismic zones, CBFs designed following a conventional design method, in which the primary requirement is for the factored resistance of all components in the lateral load path to be greater than the factored load effect, are extremely popular. Such CBFs can easily be designed by practicing structural engineers based on a linear elastic analysis using commonly available software. Moreover, the ability to waive the rigorous seismic detailing and proportioning requirements may result in structures having less steel tonnage compared to CBFs designed with capacity design principles and more stringent detailing rules, despite the higher design seismic loads (lower seismic force reduction factor) [4]. There is no dedicated seismic fuse member in these CBFs; it is assumed that sufficient seismic energy dissipation can be provided through limited yielding in members and connections along the lateral load path, as well as through friction within the joints. In this paper, such CBFs are referred to as Conventional CBFs (CCBFs). CBFs of Conventional Construction (Type CC) category in the NBCC [2] and CBFs 'not specifically detailed for seismic resistance' in accordance with ASCE /

SEI 7-16 [1] are two examples of CCBF systems. Furthermore, existing CBFs that were designed prior to the adoption of the seismic design provisions in the 1988 Uniform Building Code [5] in the USA and the CSA S16.1-M89 Standard [6] in Canada were designed for reduced seismic loads with no regard for yield and failure hierarchy, or ductile detailing [7].

Bracing members are usually connected to other framing members by means of gusset plates. The focus of most past studies on brace connections has been placed on the design of the gusset plates, e.g. Chakrabarti & Bjorhovde [8], Lehman et al. [9] and Fang et al. [10]. However, another zone can be identified within the global brace connection, that is, the brace-to-gusset connection [11]. The bracing members, brace-to-gusset connections, and gusset plates work in series along the lateral load path. Under the conventional design principle, the brace-to-gusset connection is usually the weakest link, and thus is vulnerable to fracture when the brace is subjected to tension, because the compressive buckling resistance generally governs the design and selection of the bracing members and gusset plates. Greater tensile overstrength exists in the bracing members and gusset plates compared to the brace-to-gusset connection. The brace-to-gusset plate weld deficiency in CCBFs was found experimentally and proved highly detrimental for the drift capacity by Sen et al. [12]. Brace connection failures were also reported frequently in post-earthquake reconnaissance [13,14].

Unlike many structural steel members, which usually demonstrate a minimum level of ductility prior to failure, some failure modes of the brace connections, e.g. weld failure or bolt rupture, have very limited deformation capacity. Moreover, due to the low redundancy of CBFs, the failure of brace connections may severely diminish the structural integrity, i.e. very likely cause a soft-storey mechanism, and eventually lead to structural collapse [13].

Without a predefined yield and failure hierarchy in the design process, theoretically any failure mode could occur in CCBFs under a severe seismic event, resulting in high variance and unpredictability in the structural ductility and seismic performance. Recent research on CCBFs has revealed the high risk of their seismic behaviour and has indicated that brace connections are vulnerable to failure [15,16]. In order to prevent premature brace connection failure and early loss of structural integrity, the CSA S16 Standard [17] requires that the design seismic force for brace connections be amplified by 1.5 unless ductile connection behaviour can be guaranteed. Unfortunately, due to a lack of research on this issue, no code prescribed guidelines outlining how to achieve ductile connection behaviour are readily available.

I-shape sections are very common as bracing members, because they are available with a wider range of sizes compared to hollow structural sections (HSSs). However, the connection mechanism between an I-shape brace and its gusset plates is more complex than that of HSSs. A typical I-shape brace connection configuration is the flange plate connection, as shown in Figure 1. Although commonly specified in practice, the behaviour and performance of the I-shape brace connections are far from being well understood, which poses a high risk in the seismic performance of buildings using such connections. In order to gain insight into the behaviour of typical I-shape brace connections and to propose design guidelines to achieve ductile connection behaviour of CCBFs, a coordinated experimental and analytical research project was launched at McGill University and Polytechnique Montréal [18-21]. The study presented in this paper is a continuation of this research project.

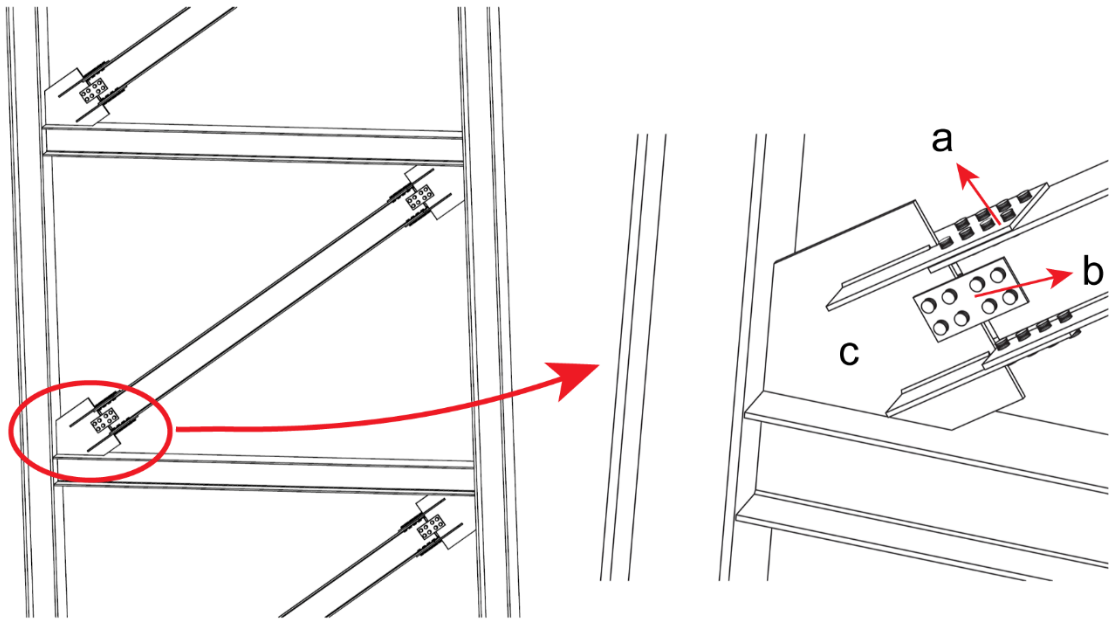

Figure 1 Schematic illustration of CCBF with I-shape braces and flange plate brace connections: (a) flange lap plate (FLP); (b) web lap plate (WLP); (c) gusset plate

A parametric study was conducted on the flange plate connection utilizing the validated finite element (FE) modelling procedure [21]. The specimens tested in the laboratory by Rudman et al. [18,19] served as the reference cases. Two I-shape sections were selected as the bracing members, to investigate the possible influence of section size. Three parameters, namely, gusset plate thickness, flange lap plate thickness, and web lap plate thickness, were varied, and their effects on both the tensile and compressive behaviour of the brace-connection assembly were studied. Recommendations are made based on the results of the parametric study, with the objective of achieving ductile behaviour of CCBFs.

2. Research project on I-shape brace connections

Currently, due to the lack of data on the seismic behaviour of CCBFs and the lack of code prescribed guidelines on how to attain ductile connection behaviour, practicing engineers in

Canada will typically resort to the use of the 1.5 amplification factor in determining the seismic design forces for brace connections (Cl. 27.11 CSA S16 [17]). This factor is equal to the ductility-related seismic force reduction factor, R_d, specified for CCBFs in the NBCC [2], with the objective of ensuring that the brace connections would remain essentially elastic under design level ground motions having a return period of 2475 years. A research project has been launched to investigate the seismic behaviour of CCBFs with I-shape braces. The objectives of this project include: to understand the behaviour of typical I-shape brace connections; to determine the force and deformation demands on brace connections; and eventually to propose design guidelines to achieve adequate structural seismic performance of CCBFs.

Under the research project, Rudman et al. [18, 19] and Wang et al. [20] conducted a series of full-scale tests on the assemblies of I-shape braces and brace connections subjected to reversed cyclic loading (Figure 2). Two brace connection configurations were tested—the flange plate connection and the flange angle connection. The assemblies were designed following conventional design principles without extra strengthening of the brace connections. As expected, highly variant behaviour was witnessed with different buckling modes, failure modes, and deformation capacities. However, even though the 1.5 force amplification was not applied in the design of these test specimens, all tested connections exhibited a measurable ductile response.

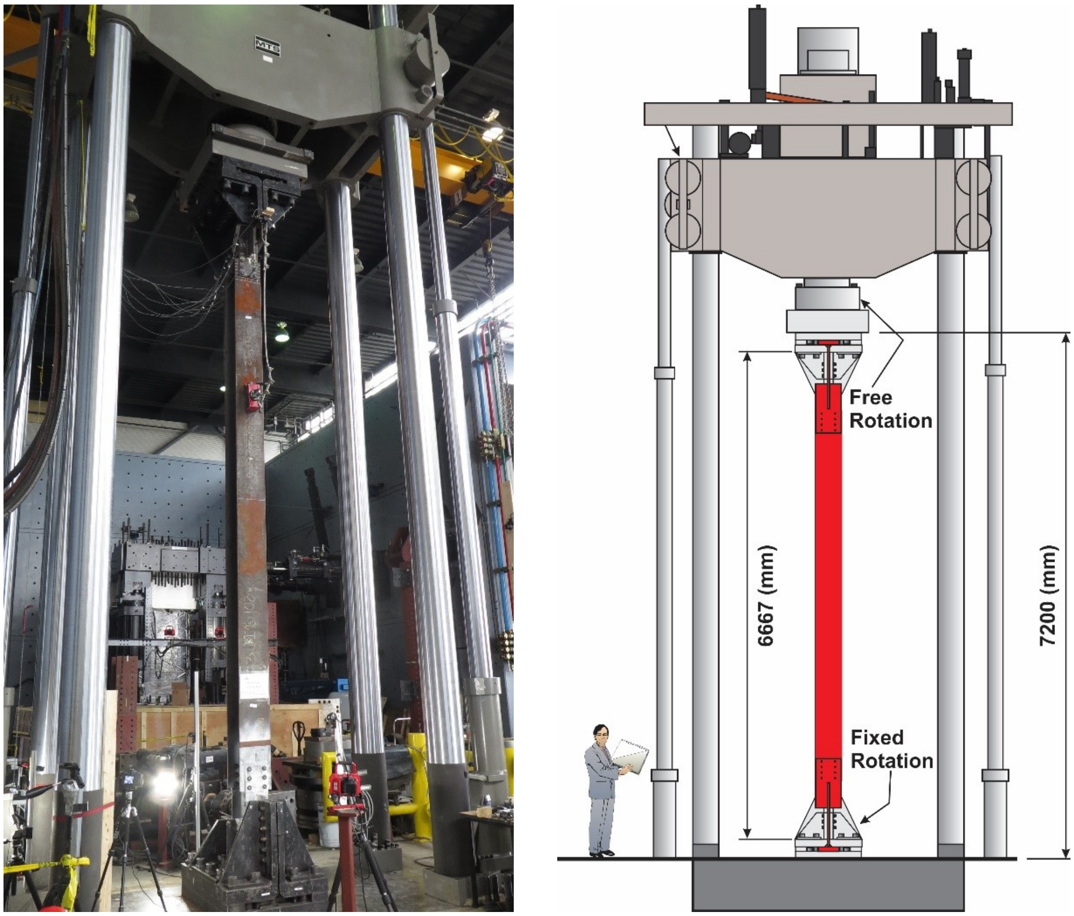

Figure 2 Test set-up of the full-scale I-shape brace and connection assembly [18,19]

A numerical simulation procedure based on 3D continuum elements was then developed by Wang et al. [21] for the flange plate brace connection. A typical FE model is shown in Figure 3. By making use of the axisymmetry, only half of the assembly was modeled for computational efficiency. The general-purpose 3D brick elements C3D8R in Abaqus were used to model most parts, except fillet welds and the K zones of braces for which wedge elements (C3D6) were used to facilitate regular meshes. The results of the steel tension coupon tests [18] were used as the input of material properties. Three types of contacts were modeled: contact between the connected plates, contact between the bolt shank and the bolt hole, and contact between the bolt nuts and the connected plates. The 'hard contact' feature in ABAQUS was used to reproduce the normal behaviour of each contact and to eliminate penetration; for the tangential contact behaviour, the friction coefficient of 0.33 was applied to capture the frictional response. In the simulations, the movements of the two ends were coupled to the two reference points through kinematic coupling, RF1 and RF2, respectively. The axial loading was realised by fixing RF2 and enforcing displacement of RF1 along the longitudinal axis of the brace. For more details about the numerical model, please refer to [21].

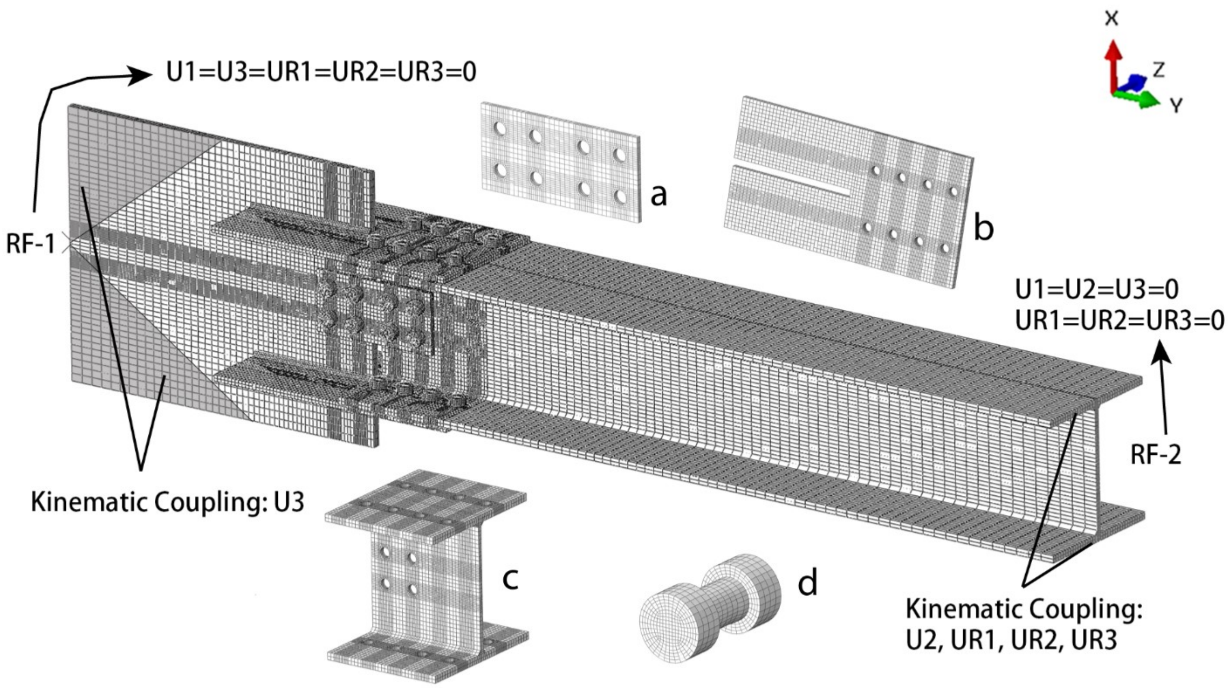

Figure 3 FE model of the brace and connection assembly by Wang et al. [21]: (a) web lap plate; (b) flange lap plate; (c) brace end with refined mesh; (b) bolt

The accuracy of the model was validated through comparison with the experimental test results [21]. The comparison of the experimental and simulated loading responses for two representative specimens is presented in Figure 4. Based on the numerical simulation results, the force transfer mechanism was studied. In order to prevent bolt shear rupture and weld fracture, which are known to have little deformation capacity, it was recommended to design the bolts and welds in the flange and web branches based on the ultimate strength of the branch, so as to achieve more ductile limit states such as bearing or yielding of the lap plates. The study also revealed a nonuniform shear force distribution within bolt groups and an eccentric loading condition for the welds connecting the flange lap plates to the gusset plates. Recommendations were also made that these effects be explicitly accounted for in design to avoid premature failure of the bolts and welds. Moreover, the validated numerical procedure laid the foundation for this parametric study on the flange lap plate brace connection.

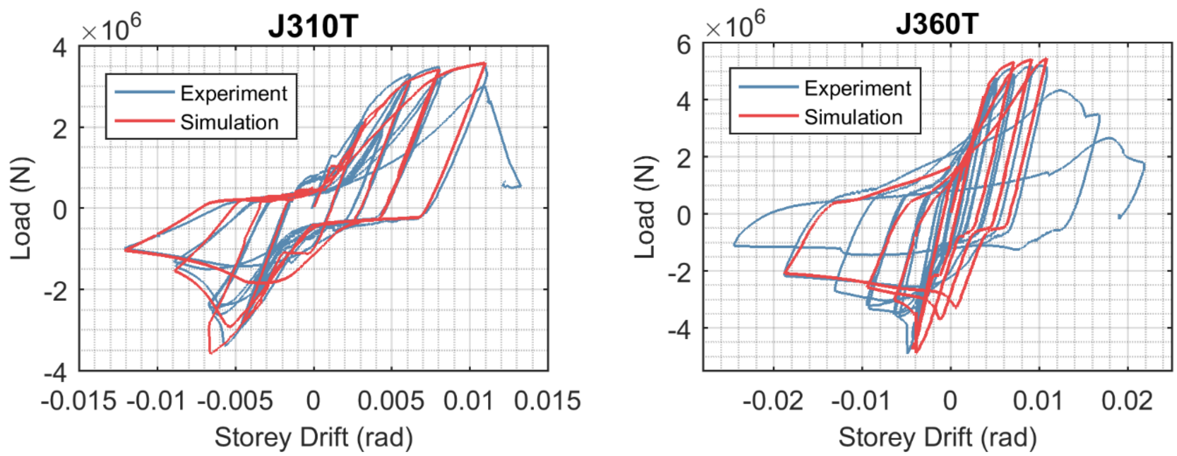

Figure 4 Comparison of experimental and simulated load vs. corresponding storey drift hysteretic curves [21]

3. Parametric study

Based on the validated FE model of the brace and connection assembly (Figure 3) by Wang et al. [21], a parametric study was conducted and presented herein. Please note that the length of the brace-connection assemblies was extracted from a prototype one-bay one-storey braced frame that was 3.75 m high and 5.5 m wide. For direct perception of the axial deformation level of the brace-connection assembly, the deformations were expressed as the corresponding storey drifts of the prototype braced frame throughout this paper. The "load" hereafter refers to the axial load applied on the brace-connection assembly.

3.1. Flange plate connection study matrix

As shown in Figure 5, the studied brace connection consists of three types of plates: flange lap plate (FLP), web lap plate (WLP), and gusset plate. In realistic designs, the relative strengths vary among the three parts, which might result in different failure modes. To study the effect of the relative strength variation, three parameters (namely, the gusset plate thickness, the FLP thickness, and the WLP thickness) were varied individually in this parametric study. The two models by Wang et al. [21] served as the reference cases, and are labeled as J310-REF and J360-REF, respectively. Four variations were considered for each parameter: 50%, 75%, 125%, and 150% relative to the quantity in the reference models. Due to the fact that the 50% variations of gusset plate thickness caused numerical convergence problems, the 65% and 60% variations were instead adopted for gusset plate thickness with respect to J310-REF and J360-REF, respectively. Therefore, twenty-six numerical models were created in this parametric study as listed in Table 1.

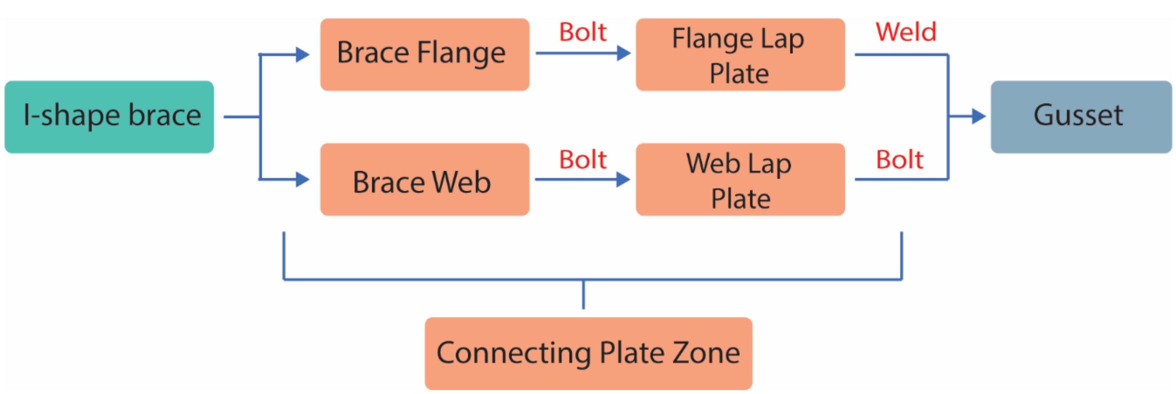

Figure 5 Main component and load path of I-shape brace flange plate connections

For the model labelling scheme, the first part indicates the reference model on which the new model was built. This is followed by letter 'G', 'F', or 'W' to indicate the component for which the thickness was varied: gusset plate, flange lap plate, or web lap plate, respectively. The final three-digit number denotes the ratio (in percentage) of the component's thickness to that of the control model. For instance, 'J310-F-125' corresponds to the model that was built on J310-REF but with the flange lap plate thickness 125% to that of the reference model.

Table 1 Flange plate connection parametric study list

Model ID	Brace Section	Bolt Grade and Size (in.)	Gusset Thickness (mm)	Flange Lap Plate Thickness (mm)	Web Lap Plate Thickness (mm)
J310-REF	W310×97	A325 (7/8)	15.9	15.9	9.53
J310-G-065	W310×97	A325 (7/8)	10.3	15.9	9.53
J310-G-075	W310×97	A325 (7/8)	11.9	15.9	9.53
J310-G-125	W310×97	A325 (7/8)	19.8	15.9	9.53
J310-G-150	W310×97	A325 (7/8)	23.8	15.9	9.53
J310-F-050	W310×97	A325 (7/8)	15.9	7.94	9.53
J310-F-075	W310×97	A325 (7/8)	15.9	11.9	9.53
J310-F-125	W310×97	A325 (7/8)	15.9	19.8	9.53
J310-F-150	W310×97	A325 (7/8)	15.9	23.8	9.53
J310-W-050	W310×97	A325 (7/8)	15.9	15.9	4.76
J310-W-075	W310×97	A325 (7/8)	15.9	15.9	7.14
J310-W-125	W310×97	A325 (7/8)	15.9	15.9	11.9
J310-W-150	W310×97	A325 (7/8)	15.9	15.9	14.3
J360-REF	W360×134	A490 (1)	19.1	15.9	9.53
J360-G-060	W360×134	A490 (1)	11.4	15.9	9.53
J360-G-075	W360×134	A490 (1)	14.3	15.9	9.53
J360-G-125	W360×134	A490 (1)	23.8	15.9	9.53
J360-G-150	W360×134	A490 (1)	28.6	15.9	9.53
J360-F-050	W360×134	A490 (1)	19.1	7.94	9.53
J360-F-075	W360×134	A490 (1)	19.1	11.9	9.53
J360-F-125	W360×134	A490 (1)	19.1	19.8	9.53
J360-F-150	W360×134	A490 (1)	19.1	23.8	9.53
J360-W-050	W360×134	A490 (1)	19.1	15.9	4.76
J360-W-075	W360×134	A490 (1)	19.1	15.9	7.14
J360-W-125	W360×134	A490 (1)	19.1	15.9	11.9
J360-W-150	W360×134	A490 (1)	19.1	15.9	14.3

3.2. Material properties

To prevent bolt rupture and weld fracture, the previous study [21] recommended the following: the bolts and welds in the flange branch of the brace connection be designed based on the ultimate tensile strength of the flange branch; the bolts in the web branch be designed based on the ultimate tensile strength of the web branch. This recommendation was subsequently proved to be effective to keep the bolts essentially elastic [21]. The parametric study presented in this paper assumes this recommendation has been implemented in the brace connection design, and hence bolts and welds would remain essentially elastic. Therefore, in this parametric study, the bolts and welds were modeled as elastic for the sake of time-saving and better numerical convergence.

For all the other parts, material nonlinearity was modelled. In order to ensure the modelling accuracy at large deformation levels, nonlinear steel strain hardening was taken into account through the implementation of the nonlinear kinematic hardening model provided in ABAQUS 6.14 [22]. Within the material plasticity model, the backstress, α, describes the translation of the yield surface with the plastic strain (ε^{pl}) in the stress-strain space. In this study, three backstresses were used to collectively model the steel kinematic hardening (Equation 1 and 2).

$$\alpha_k = \frac{C_k}{\gamma_k}\left(1 - e^{-\gamma_k \varepsilon^{pl}}\right) \tag{1}$$

$$\alpha = \sum_1^3 \alpha_k \tag{2}$$

The data obtained from unidirectional tension coupon tests [18] were utilised to calibrate the coefficients, C_k and γ_k, for each backstress. The values that provided the best correlation with the experimental data were adopted.

3.3. Loading protocol and analysis technique

All models were loaded monotonically both in compression and in tension. A maximum compressive deformation of 60 mm, approximately corresponding to 2% storey drift for the prototype frame (5.5 m wide and 3.75 m high), was applied for all models, during which inelastic buckling behaviour occurred. Either 60 mm or 110 mm displacement was enforced in tension to reach the tensile ultimate limit states. The applied deformation covers and exceeds the range of deformation anticipated for CCBFs under design level earthquakes.

Different numerical solving techniques were implemented for compression and tension loading simulations based on their capability and efficiency. For the compression simulations, the implicit dynamic method was used to ease convergence in the post-buckling range. For assemblies loaded in tension, the simpler general static approach was employed.

4. Results and Discussion

4.1. Compressive behaviour

4.1.1. Effect of gusset plate thickness

The compressive load-deformation curves of simulations with gusset plate thickness variation are plotted in Figure 6. The legend of Figure 6, and of the following figures of the same type, contain values after lines of different colours that correspond to the third part of the Model ID listed in Table 1; the title of the sub-figure corresponds to the first two parts of the Model ID specified in Table 1. For instance, the yellow line followed by ‘075’ in the sub-figure with the title of ‘J310-G’, refers to the model with the Model ID ‘J310-G-075’ defined in Table 1. The two shapes (diamond and circle) denote the two compressive buckling modes, brace buckling and gusset buckling, respectively.

Inelastic buckling with degrading compressive strength in the post-buckling range occurred in all models, in the form of either gusset plate buckling or out-of-plane brace buckling. As shown in Figure 7, the reference models J360-REF and J310-REF exhibited gusset buckling and out-of-plane overall minor-axis brace buckling, respectively, which matched with the laboratory test observations [18,19]. This drastic difference in response is expected for CCBFs as current code provisions do not stipulate a preferred buckling mode nor do they contain design rules to ensure a certain buckling mode. Hence, either form of buckling can occur, depending on the selection and detailing of the brace and its connections, as the buckling mode is determined by the relative compressive strength of the two components. The results of the FE simulations in Figure 6 show that the buckling mode was clearly affected by the gusset plate thickness: for both braces studied, the buckling mode shifted from gusset buckling to overall minor-axis brace buckling when the gusset plate thickness was increased. For specimens with brace section W310×97, the buckling mode changed from gusset buckling to overall minor-axis brace buckling with the gusset plate thickness changed from 11.9 mm to 15.9 mm; the same buckling mode shift occurred for specimens with brace section W360×134 as gusset plate thickness increased from 19.1 mm to 23.8 mm.

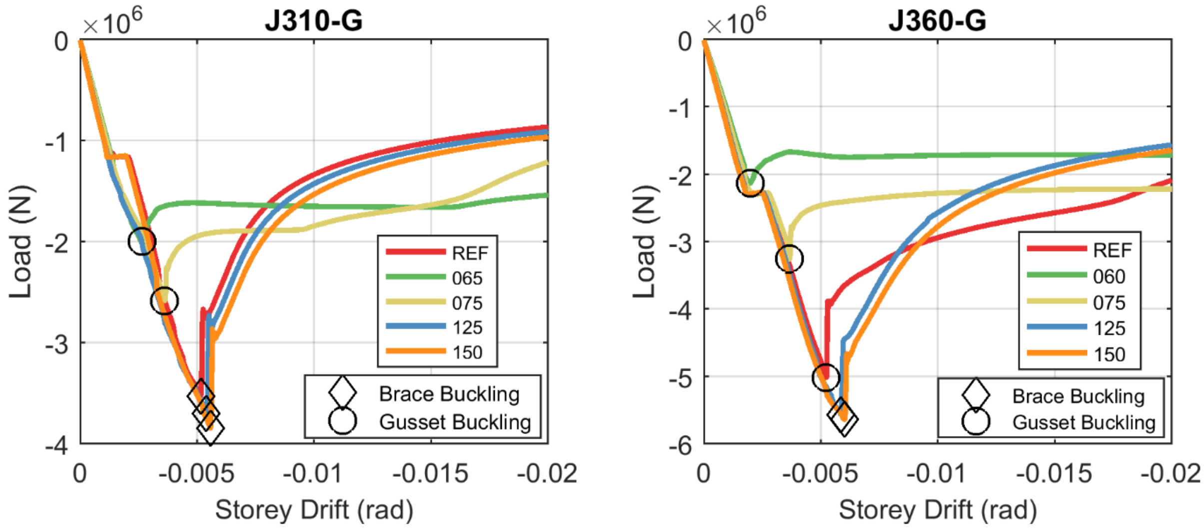

Figure 6 Compressive load-deformation curves of models with varying gusset plate thicknesses

The gusset buckling resistance was significantly affected by its thickness, which is consistent with numerous past studies on the gusset plate compressive resistance, e.g. Yam et al. [23,24]. For instance, compared to that of J360-G-060, the gusset plate buckling resistance increased by 52.6% and 135% in J360-G-075 and J360-REF, respectively. Likewise, an increase of 15.4% in gusset plate thickness resulted in a 29.3% increase in the gusset buckling resistance in the analysis of the J310-G-065 S310-G-075 assemblies.

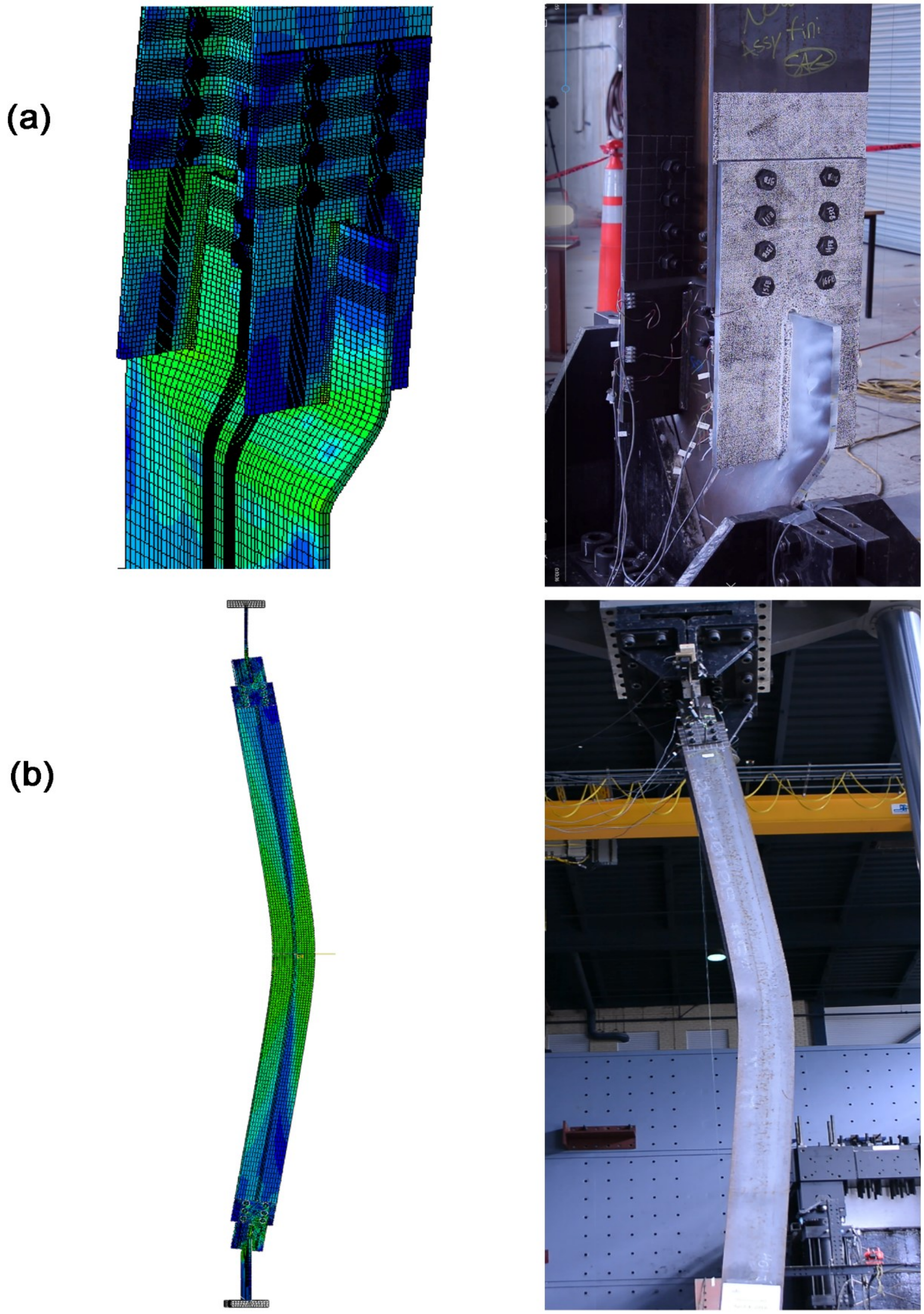

Figure 7 (a) gusset buckling in J360-REF; (b) overall minor-axis brace buckling in J310-REF

On the other hand, in the case of brace buckling, the variation of the gusset plate thickness had a less significant, yet still noticeable impact on the brace buckling resistance. For instance, the buckling resistance increased by 9.4% when changing the gusset plate thickness from 15.9 mm in J310-REF to 23.8 mm in J310-G-150. This is attributed to the increased rotational restraint provided by the greater gusset plate bending stiffness mobilized upon brace buckling [25], which will be further discussed in Section 4.1.4.

4.1.2. Brace buckling versus gusset buckling

For CBFs other than the CCBF studied in this paper, the seismic design codes generally require that energy dissipation be facilitated by the buckling of the braces in compression, along with the yielding of the braces in tension, e.g. SCBFs and OCBFs in AISC 341-16 [26] and type MD and LD CBFs in CSA S16 [17]. Gusset plate buckling is explicitly not permitted in such CBFs. However, for CCBFs, specifically the R=3 CBF system in ASCE/SEI 7-16 and type CC CBFs in CSA S16 [17], there exist no requirements with respect to the compression buckling mode, and as such, either form of instability could occur.

The results of the parametric study indicate that brace buckling should be the preferred buckling mode in order to improve CCBF seismic performance for two main reasons. Firstly, smaller plastic strain will be introduced in components by brace buckling compared to gusset buckling, resulting in a longer low-cycle fatigue life. In the case of brace buckling, axial compression deformations of the brace-connection assembly are accommodated by the bending of the brace over its entire length. In contrast, when gusset plate buckling occurs, compression deformations concentrate in the short laterally unsupported region of the gusset plate. As shown in Figure 8, at the same axial compression deformation level corresponding to 2% storey drift, the maximum plastic strain induced by gusset buckling is more than two times that imposed by brace buckling.

Note, all comparisons with percent storey drift herein are based on the prototype frame (5.5 m wide and 3.75 m high) considered by Rudman et al. [19] in their brace test program.

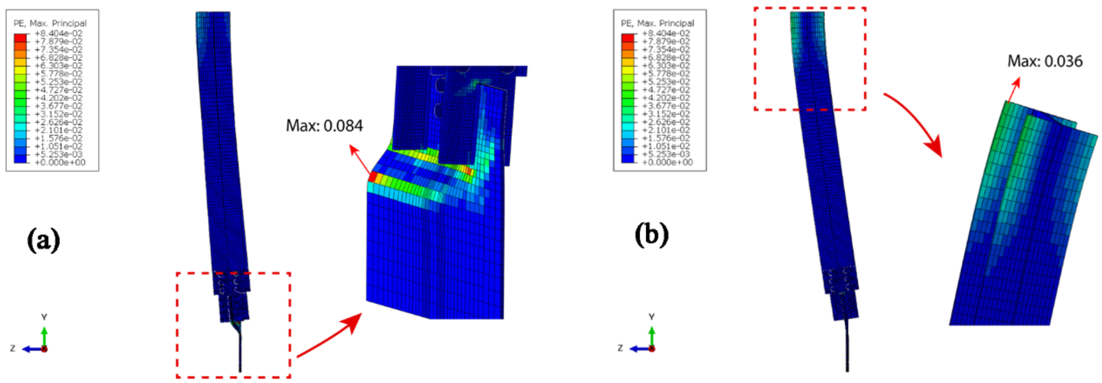

Figure 8 Maximum equivalent plastic strains induced by buckling: (a) gusset buckling in J310-G-075; (b) brace buckling in J310-REF

Secondly, gusset plate buckling is expected to occur at one end of the brace despite the nominally identical design at both ends. The variability in the buckling resistances offered by the gusset plates at the two ends of the brace, due to unavoidable differences in material properties, geometric dimensions, etc., is sufficient to trigger buckling of only one gusset plate. The subsequent compressive strength degradation will limit the force imposed on the other gusset, which results in the inelastic demands being concentrated in the gusset plate where buckling first occurred.

Walbridge et al. [27] reported on the energy absorption characteristics of gusset buckling, and proposed that the gusset plates in braced frames be the weak element in compression, rather than the braces. They observed the post-buckling resistance of the gusset plates to be stable, whereas the post-buckling resistance of the braces showed substantial degradation. However, this recommendation for weak gusset plate design did not account for the longer low-cycle fatigue life and larger axial deformation capacity characteristic of overall brace buckling. In the context of improving the seismic performance of CCBFs, it is believed that the cyclic fracture life and the inelastic deformation capacity are more critical response parameters than the energy dissipation efficiency, suggesting that brace buckling should represent the preferred inelastic mechanism under compression for this system.

4.1.3. Effect of flange lap plate thickness

The variability in the flange lap plate thickness seems not to have an impact on the buckling mode of the brace-connection assembly (Figure 9), as long as premature buckling does not occur in the flange lap plates. The models of the J310 series (J310-F-075, J310-F-125, and J310-F-150) all exhibited brace buckling. Similarly, varying the flange lap plate thickness did not change the buckling mode in the J360 series: gusset buckling occurred in J360-REF, J360-F-075, J360-F-125, and J360-F-150. However, the thinner flange lap plates failed by buckling, as shown in Figure 10. Such a buckling behaviour prevents the assembly from developing its full compressive resistance potential, which is not desirable and should be avoided.

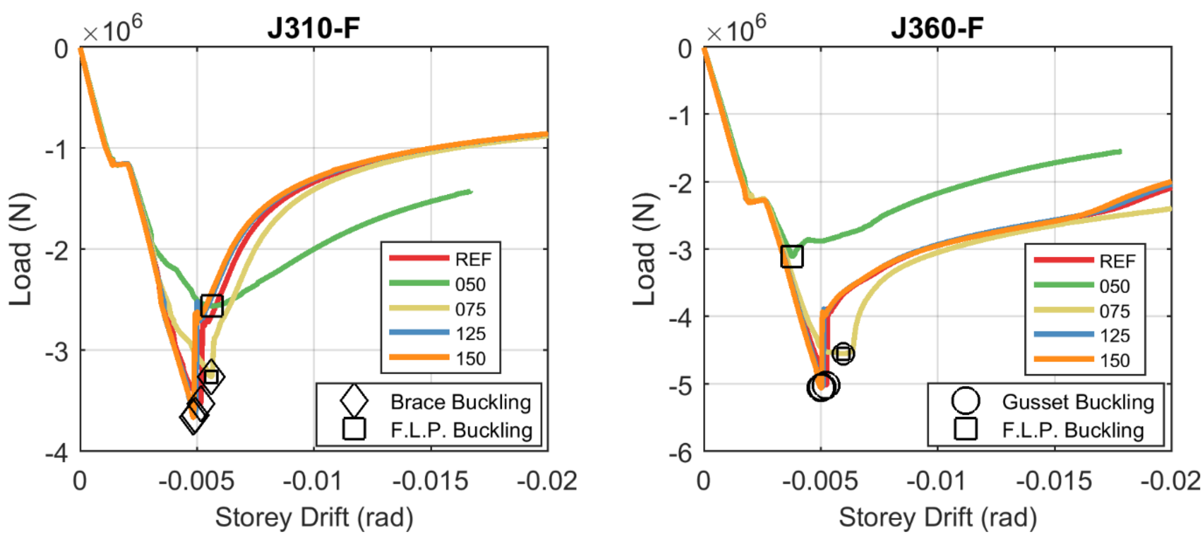

Figure 9 Compressive load-deformation curves of models with varying flange lap plate thicknesses

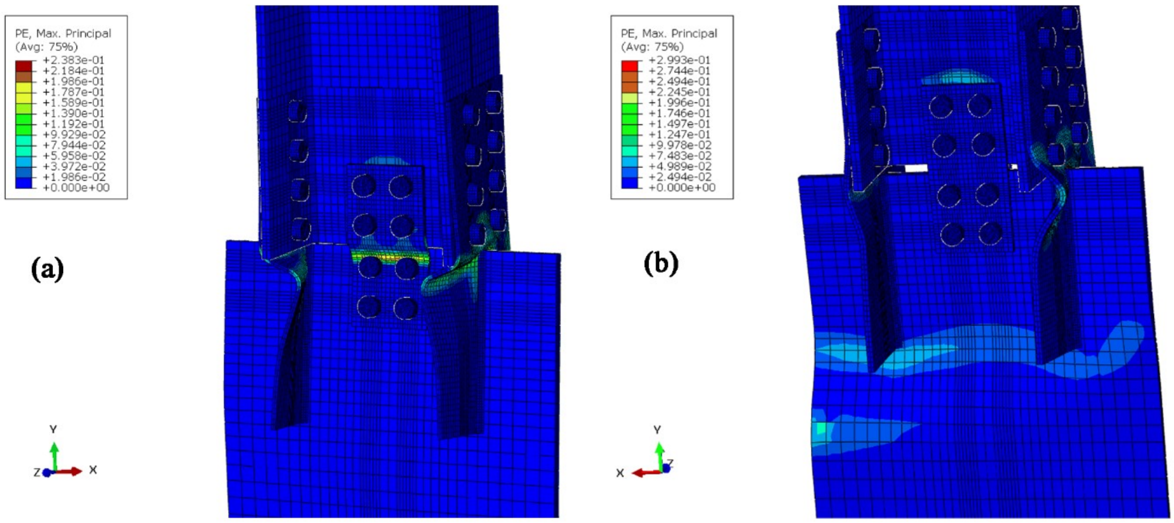

Figure 10 Compressive failure of flange lap plates: (a) flange lap plate buckling in J360-F-050; (b) Both gusset and flange lap plate buckling in J360-F-075

In terms of buckling resistance for the whole assembly, the flange lap plate thickness had different effects for the cases of brace buckling and gusset plate buckling. As shown in Figure 9, increasing the flange plate thickness led to a noticeable increase in the minor axis brace buckling resistance in the small thickness range, with values increasing from 3260 kN for J310-F-075 to 3530 kN to J310-REF; but this beneficial effect reached a plateau when thicker plates were used, with values of 3650 kN in J310-F-125 and 3660 kN in J310-F-150. Flange lap plates contribute to the end rotational restraint for the I-shape braces by means of their in-plane bending. The thicker the flange lap plates, the more restraint that is provided, and the higher the corresponding minor axis brace buckling resistance. A comparison of the plastic strain distribution in the flange lap plates at brace buckling is provided in Figure 11. The reduction of the plastic strains and the resulting greater rotational end restraint explain the increase in brace buckling resistance. Nevertheless, at a certain thickness the flange lap plates remain essentially elastic at brace buckling, as in the case of J310-F-125. Further strengthening of the flange lap plates then has limited effect on the brace buckling resistance, as in the case of J310-F-150.

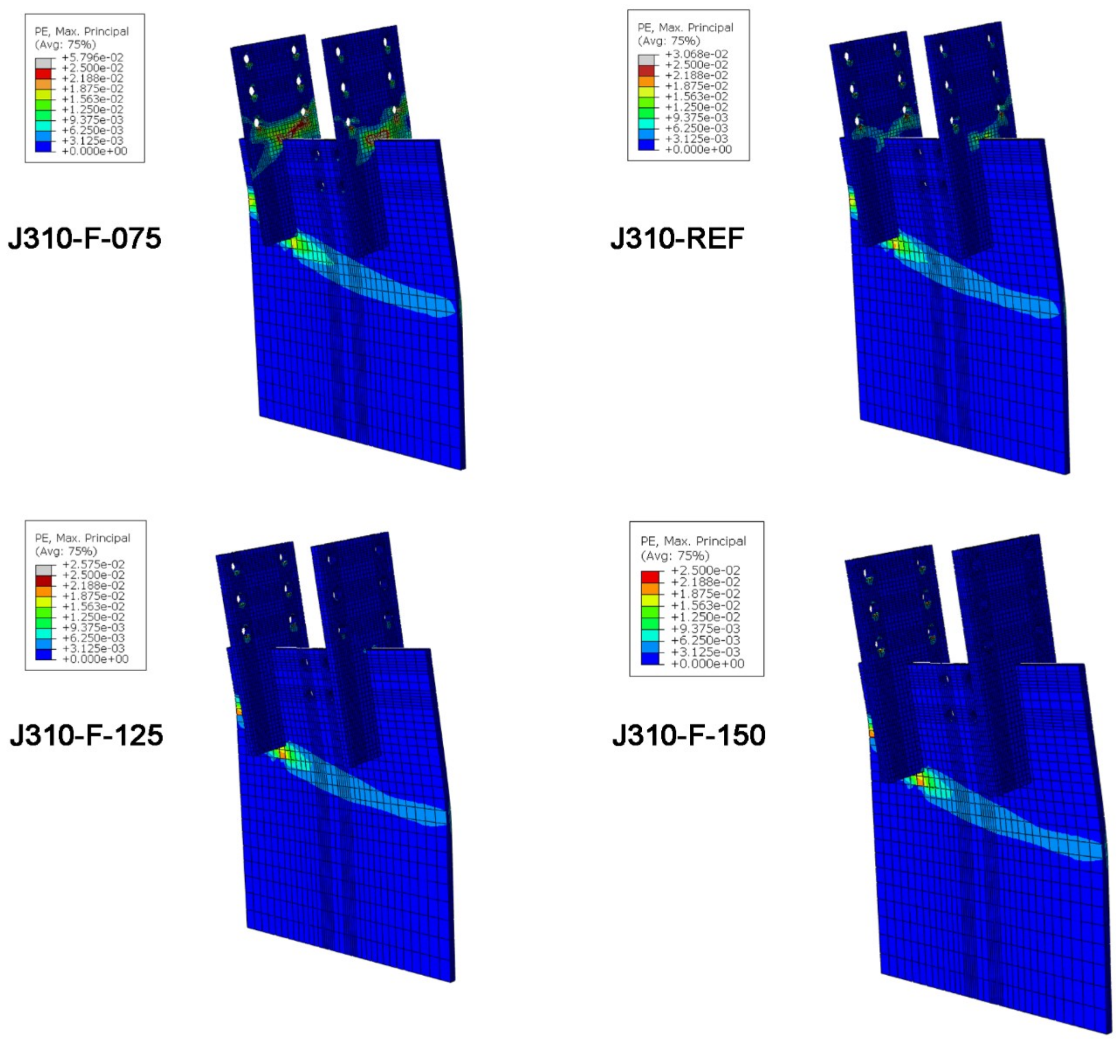

Figure 11 Comparison of plastic strains in flange lap plates at brace buckling

In the case of gusset plate buckling, the buckling resistance was not significantly affected by the thickness of the flange lap plates when flange lap plate buckling did not occur. Compressive resistances of 5015 kN, 5043 kN, and 5061 kN were obtained for J360-REF, J360-F-125, and J360-F-150, respectively. In these cases, the flange lap plates served more as orthogonal stiffeners, and the gusset plate buckling strength was determined mainly by their unstiffened lengths [28].

4.1.4. Brace effective length factor

Due to the unique geometry characteristics of the flange plate connection, the minor axis of the I-shape brace is aligned with the plane of the braced frame, and therefore, brace buckling occurs out of the plane of the frame. The analyses described in Sections 4.1.1 and 4.1.3 have revealed that the gusset plate and the flange lap plates collectively provide boundary rotational restraint for minor axis buckling of the brace. In design practice, the brace effective length (KL) is generally estimated assuming that the brace ends are pin-connected (K=1.0), and the length is taken as the distance between the expected hinge locations, L_H, as shown in Figure 12(a). However, this assumption is more suitable for the case where a distinct hinge zone is created in the gusset plate by leaving a clear distance equal to two times the thickness of the gusset ($2\ t_g$) at the end of connecting elements, as shown in Figure 12(b). Such a brace connection detail has been shown to offer small rotational restraint for the brace, and can safely accommodate the rotational demand that develops upon brace buckling [25].

However, the current design provisions for CCBFs do not require this type of clear hinge zone in the gusset plate. Practicing engineers usually discard this connection detail to achieve more compact and more economical gusset plate designs, as shown in Figure 12(c). Without the ability to accommodate brace end rotation, the brace end connections provide more substantial rotational restraint for minor axis brace buckling. Not accounting for this brace end restraint in design can lead to a low estimation of the brace buckling resistance, which may be problematic if brace buckling is the desired inelastic mechanism in compression, instead of gusset buckling. In this situation, it is possible for gusset buckling to occur during a seismic event because the braces are stronger in compression than predicted in design.

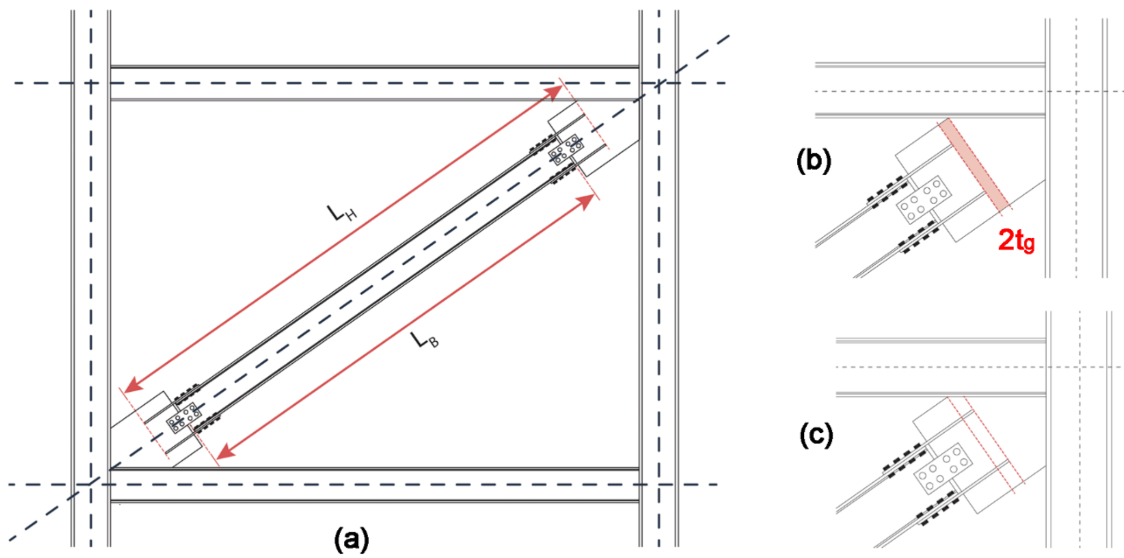

Figure 12 Gusset plate design with and without clearance in the flange plate connection

Therefore, actual support conditions of I-shape braces in CCBFs should be accounted for in the determination of the brace effective length (KL). Currently, the brace factored compressive resistance, C_r, in CSA S16-19 [17] for overall flexural buckling is calculated from:

$$C_r = \phi A F_y (1 + \lambda^{2n})^{-1/n} \tag{3}$$

in which, the brace slenderness, λ, is defined as:

$$\lambda = \frac{KL}{r}\sqrt{\frac{F_y}{\pi^2 E}} \tag{4}$$

Where ϕ is the resistance factor, A is the area of the cross section, F_y is the yield stress, n is a coefficient associated with the buckling curve, K is the effective length factor, L is the buckling length, r is the radius of gyration and E is Young's modulus. Using these equations, the effective length factor, K_{CSA}, was back-calculated using the brace buckling resistances obtained from the

FE simulations. In that calculation, L was taken equal to the I-shape brace length, L_B, as shown in Figure 12(a), and the resistance factor ϕ was set equal to 1.0. The calculations were repeated using the equations for the compressive strength of members in the AISC 360 Specification [29] to obtain the effective length factor, referred to as K_{AISC}. Input for these calculations and the resulting K factors are presented in Table 2.

Table 2 Effective length factors from brace buckling resistances obtained in FE analysis

Model ID	F_y (MPa)	E (MPa)	r_y (mm)	L_B (mm)	C_r (kN)	K_{CSA}	K_{AISC}
J310-REF	352	224000	77	5334	3530	0.74	0.80
J310-G-125	352	224000	77	5334	3700	0.67	0.70
J310-G-150	352	224000	77	5334	3850	0.59	0.61
J310-F-075[a]	352	224000	77	5334	3260	0.86	0.94
J310-F-125	352	224000	77	5334	3650	0.69	0.73
J310-F-150	352	224000	77	5334	3660	0.68	0.73
J360-G-125	355	197000	94	5067	5570	0.63	0.62
J360-G-150	355	197000	94	5067	5640	0.59	0.58

[a] Brace buckling was accompanied by flange lap plate buckling in this analysis .

As shown, the calculated brace effective length factors K_{CSA} range from 0.59 to 0.86 with a mean value of 0.68. When using the AISC 360 equations, the effective length factors K_{AISC} vary between 0.58 and 0.94 with a mean value of 0.71. Clearly, current design practice for CCBFs may lead to a significant underestimation of the minor axis brace buckling resistance. To achieve the preferred minor axis brace buckling inelastic mechanism under seismic events, it is recommended that the gusset plate be designed to resist the brace compressive resistance determined with consideration of the actual brace end conditions. Further research is needed to quantify brace effective length factors as a function of the geometrical properties of typical flange plate connections used in CCBFs.

4.1.5. Effect of web lap plate thickness

As shown in Figure 13, the FE simulations revealed that the thickness of the web lap plate had almost no impact on the buckling resistance of either the gusset plate or the brace. For the models in which brace buckling was observed, the web lap plate was bent about its minor axis. Therefore, their limited flexural stiffness and strength provided little restraint for brace buckling. In the cases where gusset plate buckling occurred, out-of-plane displacement developed in the laterally unsupported region of the gusset; this region was usually defined by the location of the flange lap plates. Because web lap plates are generally short and do not extend into the unsupported region of the gusset plates, they also have little influence on the compressive strength associated with gusset plate buckling.

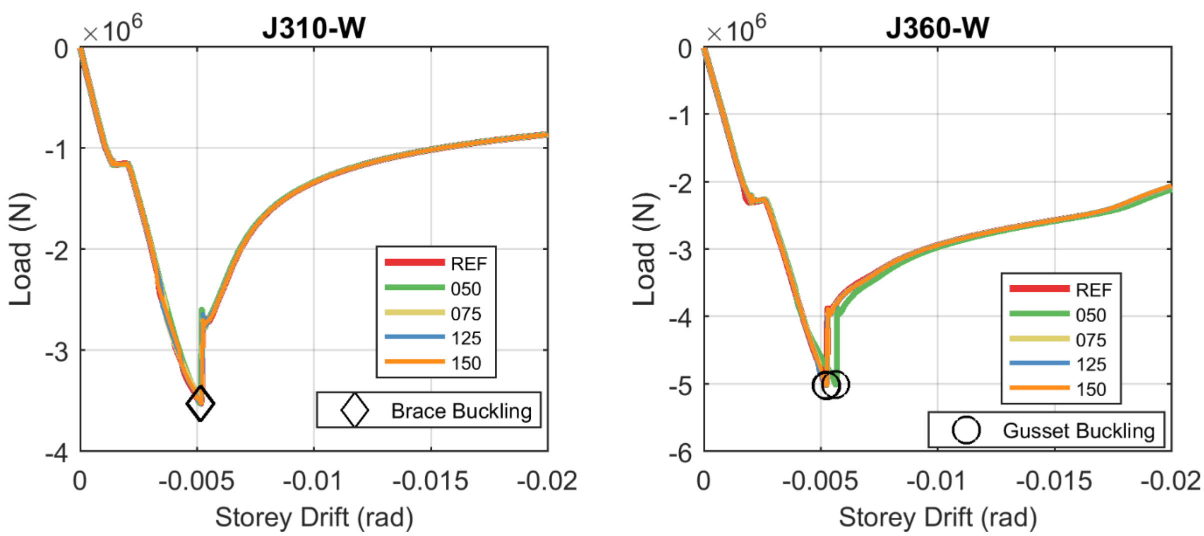

Figure 13 Compressive load-deformation curves of models with varying web lap plate thicknesses

4.2. Tensile behaviour

4.2.1. Effect of gusset thickness

The tensile load-deformation curves of all models with varying gusset plate thicknesses are plotted in Figure 14. The ultimate tensile resistances of each model, calculated in accordance with CSA S16 [17] using measured material properties and a resistance factor equal to 1.0, are also plotted for comparison (dashed lines). The failure occurred either in the gusset plate (gross section fracture) or in the connecting plate zone (net-section fracture of the flange lap plates and block shear failure of the brace web, as shown in Figure 15). The calculated CSA S16 resistances match well the ultimate tensile resistances predicted by FE simulations, except that the CSA S16 equations gave lower values than the FE simulations for cases where failure occurred in the connecting plate zone. Those cases will be discussed in detail in Section 4.2.3.

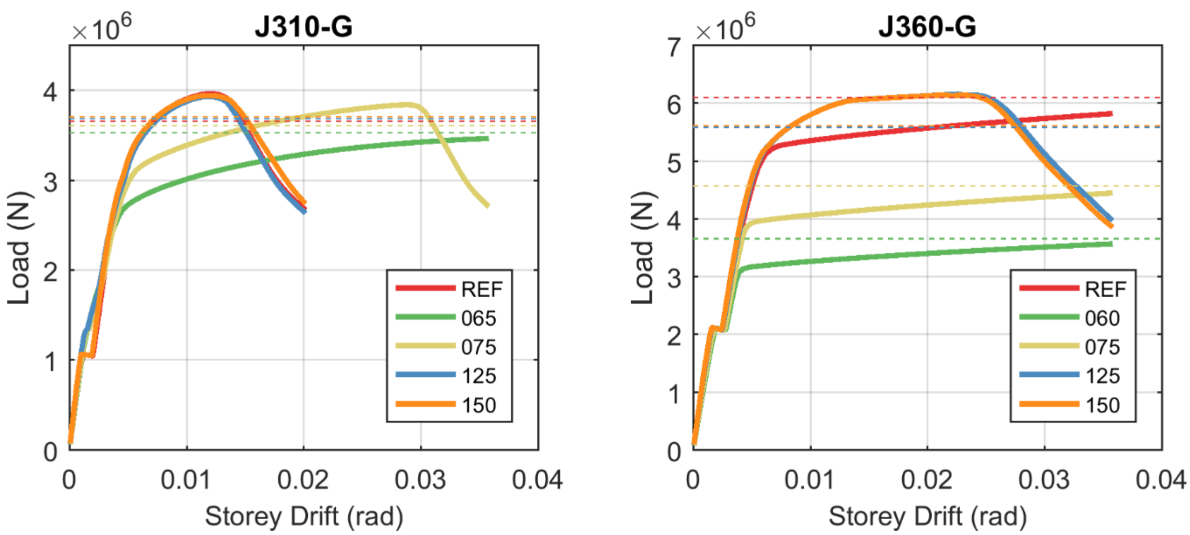

Figure 14 Tensile load-deformation curves of models with varying gusset plate thicknesses

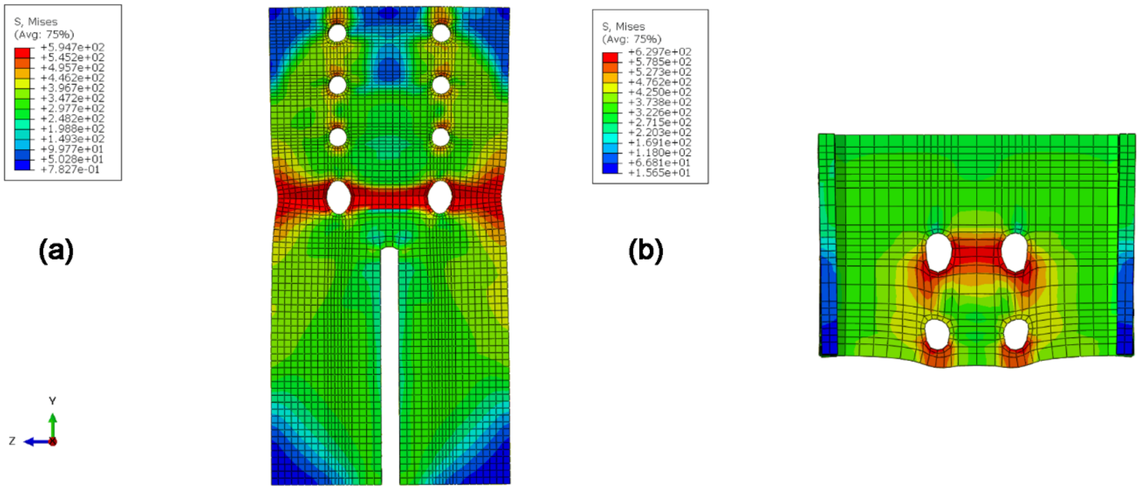

Figure 15 Failure modes in the connecting plate zone: (a) net-section fracture of flange lap plate; (b) brace web block shear

The ultimate tensile strength was governed by the connecting plate zone in J310-G-075 and J310-REF. However, for these two models, the resistance began to deteriorate at deformations corresponding to storey drifts of 1.3% and 2.8%, respectively, due to the necking of the flange lap plates. If the deformation at which resistance degradation starts due to necking of the plate is taken as the deformation capacity of the assembly, which is reasonable since there is little deformation reserve beyond that, model J310-G-075 had better deformation capacity than J310-REF. This is because the ultimate tensile strength of the connecting plate zone was larger than the yield strength of the gusset plate in model J310-G-075. As such, the gusset plate yielded before the connecting plate zone reached its ultimate strength, which contributed substantially to the global deformation of the assembly. In contrast, the gusset plate remained essentially elastic in model J310-REF, contributing little to the global deformation; almost all deformation concentrated in the connecting plate zone. The gusset plates also remained elastic in models J310-G-125 and J310-G-150, which explains why these two models showed almost the same global deformation as J310-REF. Therefore, from the perspective of deformation capacity of the

CCBFs, having stronger gusset plates is not necessarily beneficial, as it may force the plastic deformations to concentrate in the connecting plate zone.

J360-G-150 and J310-G-150 shared two similarities: their ultimate tensile strengths were governed by the connecting zone and almost all deformations concentrated in the connecting plate zone due to very strong gusset plates. However, the tensile resistance declined at deformation levels corresponding to storey drifts of 2.6% and 1.3% in models J360-G-150 and J310-G-150, respectively, due to necking in the flange lap plates. The assembly deformation at which the resistance starts to decline is indicative of the ductility of the assembly. The large difference in the tensile deformation capacities for these two models can be due to differences in the flange lap plate properties, such as the bolt gauge, the end edge distance, and the net-to-gross area ratio in the net section. Further research is needed to better understand the relation between the flange lap plate deformation capacity and its geometrical properties.

4.2.2. Effect of flange lap plate thickness

The tensile load-deformation curves (solid lines) and the calculated ultimate tensile strengths (dashed lines) according to CSA S16 [17] using measured material properties [18] and a resistance factor equal to 1.0 are provided in Figure 16. For models J310-F-125 and J310-F-150, the dashed lines represent the gross section yield strength of the brace. The code-compliant strength predictions matched well with the ultimate tensile strengths in general; nonetheless, again, for all models that failed in the connecting plate zone (J-310-REF, J-310-F-50, J-310-F-75, J-360-F-50, and J-360-F-75), the ultimate strengths calculated with CSA S16 underestimated the maximum forces developed in these models.

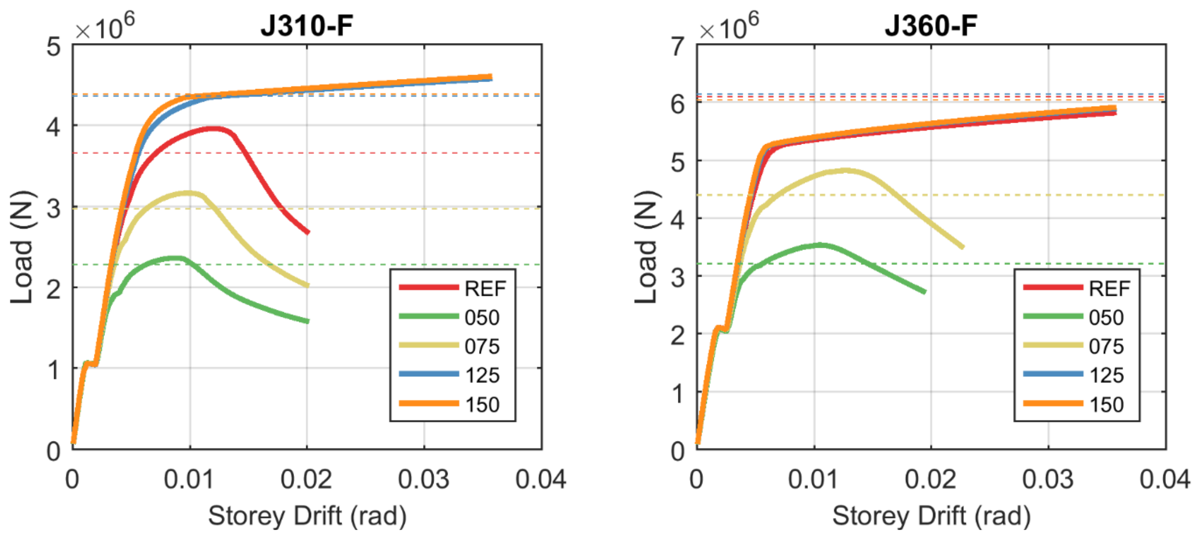

Figure 16 Tensile load-deformation curves of models with varying flange lap plate thicknesses

In the models J360-F-050 and J310-F-050, the governing failure modes were flange lap plate net-section fracture and block shear of the brace web. For these models, almost all the plastic deformations occurred in the connecting plate zones, and the lowest deformation capacities were observed.

When the flange lap plate thickness was increased, the resulting increase in the tensile resistance of the connecting plate zone forced other parts to engage plastically and to contribute more to the global deformation capacity. For instance, the ultimate tensile resistance was still governed by the connecting plate zone in J310-F-125 and J310-F-150. However, their ultimate tensile resistances were larger than the yield strength of the brace. Therefore, before these two assemblies reached their ultimate tensile strengths, the braces yielded and contributed to the global deformation, greatly improving the deformation capacity of the whole assembly. Similarly, models J360-F-125 and J360-F-150 exhibited better deformation capacities compared to J360-F-075 because strengthening of the flange lap plates made the tensile failure shift from the connecting plate zone to the gusset plates. The plastic deformations in the gusset plates improved the deformation capacity of the brace-connection assembly; and necking of the gusset plate was not observed even when the deformation had reached a value corresponding to 3.5% storey drift. However, one must note that plastic strains introduced by tensile stretching of the gusset plates may have detrimental effects on the low-cycle fatigue life of the gusset plate if the compressive failure mode is gusset buckling. In that case, inelastic tensile strains would add to plastic straining induced upon gusset buckling, which can promote premature fracture of the gusset plate. This behaviour was observed in the test J-360-T by Rudman et al. [19]. In that test, buckling of the gusset plate took plate in compression; tearing failure developed soon thereafter on a tension excursion at a relatively low deformation level in the region of the gusset plate where the buckling-induced deformations had occurred, as a result of the cumulative reversed plastic strains.

4.2.3. Overstrength of flange lap plates

As noted earlier in the text, when tension failure occurred in the connecting plate zone in the FE simulations, the strength values calculated with CSA S16 [17] always underestimated the tensile strength predicted by the FE models. A subsequent examination of the force development within the two branches of the connecting plate zone revealed that the code underestimation mainly came from the strength prediction of the flange lap plates. The CSA S16 predicted strengths of the flange lap plates (T_{u_CSA}) and the strengths obtained through FE simulation (T_{u_FEA}), as well as the resulting overstrength ratios (T_{u_FEA}/T_{u_CSA}), are given in Table 3 for models in which net-section fracture occurred in the flange lap plates.

The stress distribution within the flange lap plates under tension loading was investigated in detail. The typical distribution of all stress components when the applied load reached its maximum in the flange lap plate is shown in Figure 17. The stresses along the primary loading direction of the flange lap plate (σ_{yy}) are significant across the whole net section. In addition, substantial tensile stresses in the transverse direction (σ_{zz}) exist in the net section, between the two bolt holes. In the σ_{zz} distribution, there is also a coexisting zone (blue colour) at the upper edge of the flange plate where significant compressive transverse stresses develop. The combination of these transverse stresses results in an in-plane moment acting on the symmetry plane of the flange lap plate, over the length of the bolt group, as shown in Figure 18. This moment is caused by the eccentricity that exists between the bolt lines and the welds connecting the flange lap plate to the gusset plate.

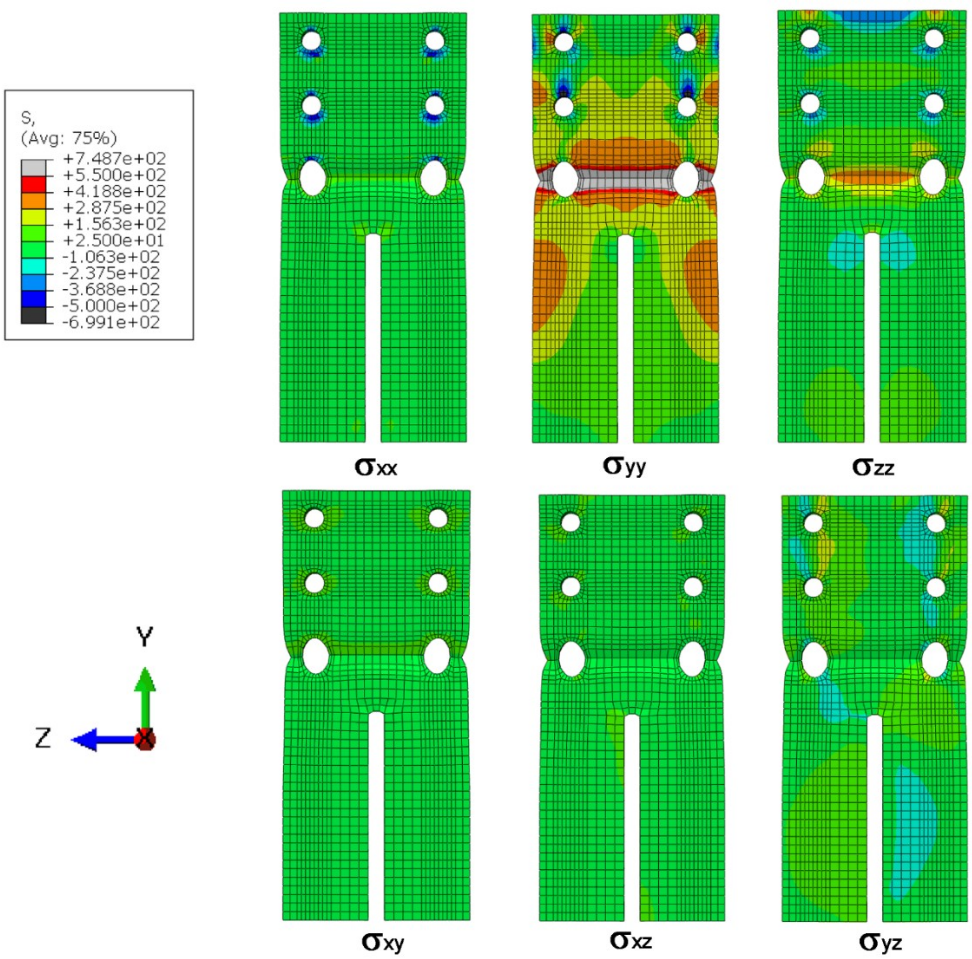

Figure 17 Stress components within the flange lap plates at the maximum tension loading

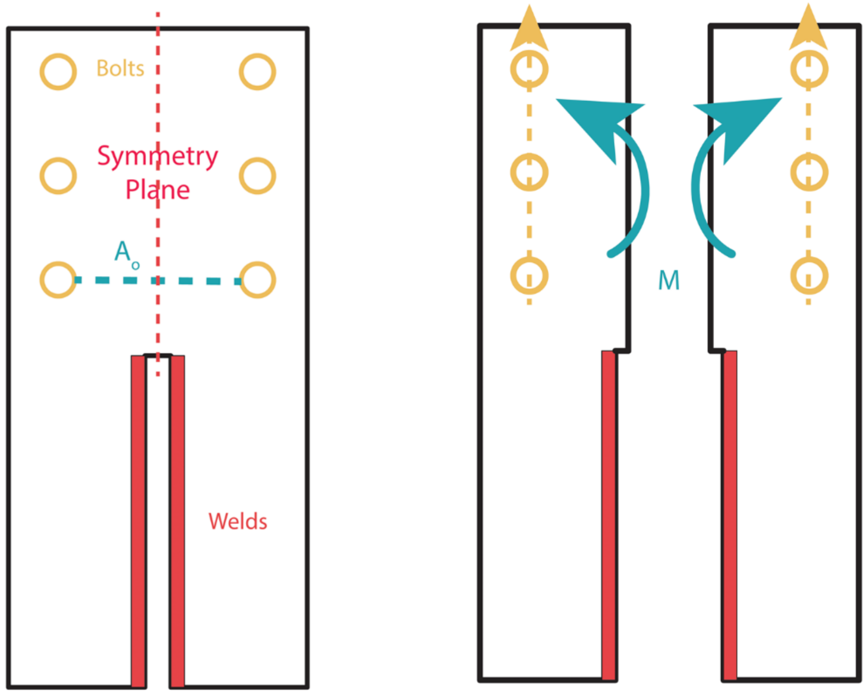

Figure 18 Schematic illustration of moment in the symmetry plane of flange lap plate

The four other stress components along the net cross section are negligible. Hence, stresses in the critical net section can be expressed as a planar bi-axial stress condition with principal stresses equal to σ_y and σ_z in accordance with the coordinate system in Figure 17. According to the von Mises yield criterion, the equivalent stress in this case is:

$$\sigma_e = \sqrt{{\sigma_y}^2 - \sigma_y \sigma_z + {\sigma_z}^2}. \quad (5)$$

For a steel with a given ultimate stress F_u, the existence of a tensile stress (+) in the Z direction (σ_z) therefore leads to an increase of the stress required in the Y direction (σ_y) to reach F_u. This increase in longitudinal stress (σ_y) at rupture on the net section due to the bi-axial stress condition is seen as the cause for the overstrength associated with net section rupture that was observed in the FE simulations compared to CSA S16 predictions. To quantify the increase of the stress, σ_y, it is assumed that the stress condition between the bolt holes is:

$$\sigma_z = x\sigma_y \tag{6}$$

Equation 5 then changes to:

$$\sigma_e = \sigma_y\sqrt{1 - x + x^2} \tag{7}$$

The square root term in Eq. 7 takes a minimum value of 0.866 when x = 0.5, which means that σ_y can attain a maximum value of 1.15 σ_e when $\sigma_z = 0.5\sigma_y$. For this condition, it is possible to determine an upper bound for the ultimate strength for net section rupture of the flange lap plates assuming that the stress σ_y at rupture is equal to 1.15 F_u on the portion A_o of the plate net section between the bolt holes (Figure 18) and F_u on the remaining of the net section $(A_n - A_o)$. Based on this assumption, the tensile overstrength ratio for the flange lap plate net section rupture, denoted herein by α_o, with respect to CSA S16 prediction, can be obtained from:

$$\alpha_o = \frac{1.15A_o + (A_n - A_o)}{A_n} \tag{8}$$

where A_n is the net section area, and A_o is the area between the bolt holes in the net section as shown in Figure 18. The ratio A_o/A_n for the J310 and J360 series of models is equal to 0.67 and 0.44, respectively. Using Equation 8, the overstrength ratios α_o for these two series are 1.10 and 1.07, respectively. These two values match well with the overstrength ratios obtained through FE simulations (Table 3).

In the previous study by Wang et al. [21], to avoid bolt shear rupture and premature weld fracture in the connection, the authors recommended that the bolts and welds of the flange lap plates be designed to resist a load equal to the tensile resistance of the flange branch. In view of this, the overstrength ratio, α_o, calculated based on Equation 8 is recommended to be used in the tensile resistance determination of the flange lap plate, which should be considered in the design of bolts and welds in the flange branch.

Table 3 Net-section overstrength of flange lap plates

Model ID	T_{u_CSA} (kN)	T_{u_FEA} (kN)	Ratio (T_{u_FEA}/ T_{u_CSA})	α_o
J310-J-075	1032	1181	1.14	1.10
J310-G-075	1377	1555	1.13	1.10
J310-G-100	1377	1572	1.14	1.10
J310-G-125	1377	1549	1.13	1.10
J310-G-150	1377	1552	1.13	1.10
J360-J-075	1779	1915	1.08	1.07
J360-G-100	2372	2465	1.04	1.07
J360-G-125	2372	2547	1.07	1.07
J360-G-150	2372	2529	1.07	1.07

4.2.4. Effect of web lap plate thickness

The tensile loading simulation results for the web lap plate thickness variation are plotted in Figure 19.

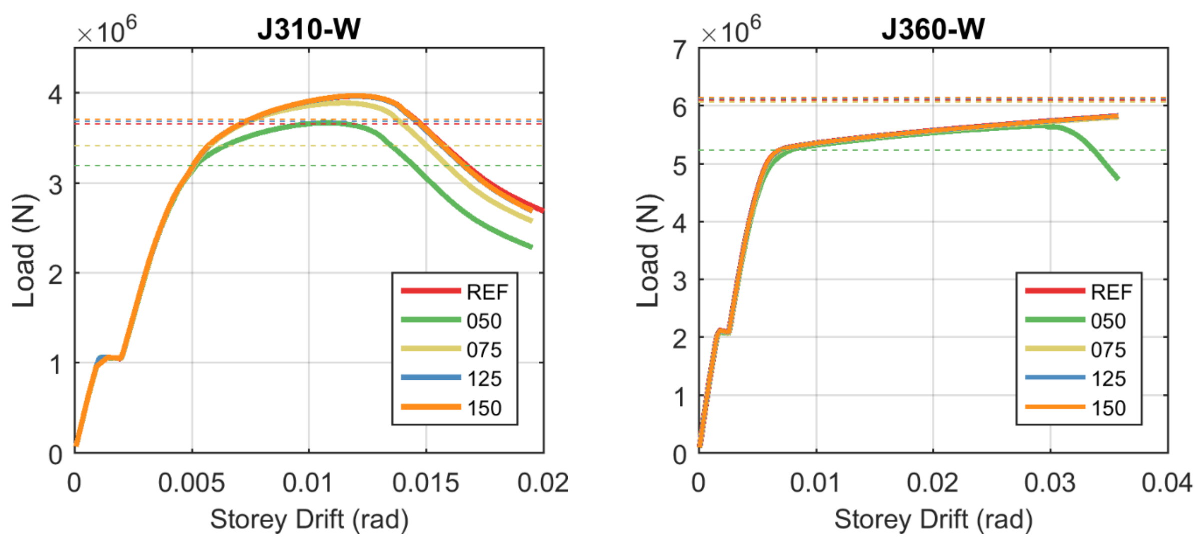

Figure 19 Tensile load-deformation curve comparison with varying web lap plate thicknesses

In the FE simulations for models J310-REF and J360-REF, block shear failure was observed in the web of the brace, as occurred in the tests by Rudman et al. [19]. When reducing the web lap plate thickness in the simulations, the failure mode shifted to net-section fracture of the web lap plates, as shown in Figure 20. Moreover, with the decrease of the web lap plate thickness, the ultimate tensile strength of the connecting plate zone decreased, and other parts (the brace and gusset plate) became relatively stronger. At the point where the ultimate strength of the brace-connection assembly was reached, the contribution of the brace and gusset plate deformations to the global deformation was therefore reduced. This explained why the resistance degradation in J310-REF and J310-W-050 occurred at deformations of 47 mm and 42 mm, equal to storey drifts of 1.5% and 1.4%, respectively. This 5 mm difference in global deformations all came from the brace and gusset plate because the flange lap plates were the same in both models. The same trend occurred in the J360 series, for which the resistance decline happened earlier in J360-W-050 than in J360-REF.

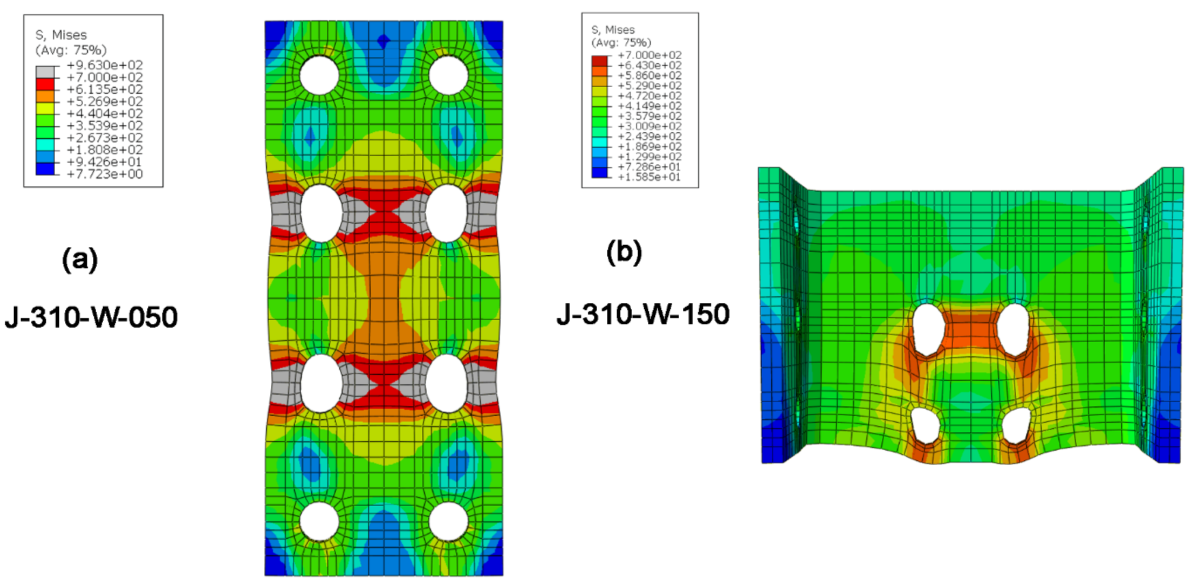

Figure 20 Failure mode shift: (a) net-section fracture in J-310-W-050; (b) brace web block shear in J-310-W-150

The tensile behaviour of models J310-W-125 and J310-W-150 was almost identical to that of J310-REF. This is because the strengthening of only the web lap plate did not change the failure modes in the web branch. Therefore, neither the tensile strength nor the deformation was changed. The same behaviour was observed when modifying the thickness of the web lap plate in the J360 model series.

5. Conclusions and Design Recommendations

A parametric study of the behaviour of the flange plate connection for I-shape braces, a configuration commonly used in CCBFs, was conducted based on a validated numerical simulation procedure. Three parameters, the gusset plate thickness, the flange lap plate thickness, and the web lap plate thickness, were varied for two different brace connection assemblies replicating specimens previously tested by Rudman et al. [19]. Both tensile loading and compressive loading were simulated monotonically. The response was examined up to large deformations exceeding the level expected under the design level seismic demand, with the focus on failure modes and deformation capacities. The primary conclusions are as follows:

1. In CCBFs with I-shape braces designed in accordance with current practice, either the gusset plates or the braces can buckle when subjected to compression. Gusset plate buckling could lead to inferior seismic performance for two reasons: a) gusset plate buckling will impose much larger plastic strains at the buckling position than brace buckling, which may lead to diminished low-cycle fatigue life for the assembly; b) gusset plate buckling is expected to occur at only one brace end due to inherent variations in material and geometric properties, which will increase further the plastic strains in areas of buckling.

2. Flange lap plates provide end restraint for both the gusset plates and the I-shape braces when subjected to compression, yet in different ways. The flange lap plates work as stiffeners for the gusset plates while offering rotational restraint through in-plane bending stiffness for the I-shape braces. Therefore, varying the flange lap plate thickness was found not to have an impact on the gusset buckling compressive resistance. However, for overall brace buckling, the use of thicker flange lap plates leads to shorter brace effective lengths and higher brace compressive resistances.
3. The end rotational restraint for the I-shape braces as collectively provided by the gusset plates and the flange lap plates can be significant in CCBFs as there is no requirement for minimum clearance to form a hinge zone in the gusset plates to accommodate the brace end rotation. The current design assumption that braces have pinned end connections can lead to a significant underestimation of the brace compressive resistance, which could result in gusset plate buckling during a seismic event.
4. Opting for a strong gusset plate design is not necessarily beneficial for the global deformation capacity because it can force plastic deformations to concentrate in the connecting plate zone. An alternative approach consisting of using thicker flange lap plates to increase the tensile resistance of the connecting plate zone will cause other components of the assembly (gusset plates or braces) to participate more in the plastic deformation in tension, which may result in higher global deformation capacities.
5. The FE simulations revealed the presence of significant transverse tensile stresses in the critical net section of the flange lap plates, which can cause an increase in the longitudinal tensile strength of these plates.

6. Modifying the thickness of the web lap plates had no impact on the compressive behaviour of the brace-connection assembly. Nonetheless, tensile failure may change from block shear of the brace web to net section failure of the web lap plates when thinner web lap plates are used."

In view of the conclusions drawn from the parametric study, the following design recommendations are proposed in order to obtain improved seismic performance of CCBFs with I-shape braces and flange plate brace connections:

1. Overall minor-axis brace buckling should be the governing buckling mode rather than gusset plate buckling.
2. The actual brace end conditions should be considered when determining the gusset plate resistance required to achieve the desired brace buckling response in compression, rather than assuming braces are pinned at both ends.
3. The connecting plate zone should be designed for a tensile axial load corresponding to the yield strength of either the gusset plate or the brace, whichever is lower.
4. The derived tensile overstrength ratio in Eq. 8 should be used in the tensile resistance determination of the flange lap plates.

Acknowledgements

The work was funded by the Natural Sciences and Engineering Research Council of Canada (NSERC), the Fonds de recherche du Québec - Nature et technologies (FRQ-NT) and the Centre d'études interuniversitaire des structures sous charges extremes (CEISCE). The financial and technical support from DPHV Structural Consultants and the ADF Group Inc. is gratefully acknowledged. The first author is supported in part through the China Scholarship Council (CSC).

The numerical simulations were conducted on the supercomputer cluster Graham of Compute Canada, which is funded by the Canada Foundation for Innovation (CFI).

References

[1] American Society of Civil Engineers/Structural Engineering Institute (ASCE/SEI) 7-16. (2016). Minimum Design Loads and associated criteria for buildings and other structures. Reston, Virginia, USA.

[2] National Research Council of Canada (NRCC). (2015). National Building Code of Canada (NBCC) (13th ed.). Ottawa, ON, Canada.

[3] Mitchell, D., Tremblay, R., Karacabeyli, E., Paultre, P., Saatcioglu, M., & Anderson, D. (2003). Seismic force modification factors for the proposed 2005 edition of the National Building Code of Canada. Canadian Journal of Civil Engineering, 30(2), 308-327. doi:10.1139/l02-111

[4] Brunet, F., Tremblay, R., Richard, J., & Lasby, M. (2019). Improved Canadian seismic provisions for steel braced frames in heavy industrial structures. Journal of Constructional Steel Research, 153, 638-653. doi:10.1016/j.jcsr.2018.11.008

[5] ICBO. (1988). Uniform building code, 1988 ed. In Proc., Int. Conf. of Building Officials. Whittier, Calif.: International Conference of Building Officials.

[6] Canadian Standards Association. (1989). CSA S16. 1-M89. Steel structures for buildings—Limit states design. Rexdale, ON, Canada.

[7] Sen, A., Swatosh, M., Ballard, R., Sloat, D., Johnson, M., Roeder, C., Berman, J. (2017). Development and evaluation of seismic retrofit alternatives for older concentrically braced frames. Journal of Structural Engineering, 143(5), 04016232-04016232. doi:10.1061/(ASCE)ST.1943-541X.0001738

[8] Chakrabarti, S., & Bjorhovde, R., F. ASCE. (1985). Tests of full-size gusset plate connections. Journal of Structural Engineering, 111(3), 667-684. doi:10.1061/(ASCE)0733-9445(1985)111:3(667)

[9] Lehman, D., Roeder, C., & Herman, D. (2008). Improved seismic performance of gusset plate connections. Journal of Structural Engineering, 134(6), 890-901. doi:10.1061/(ASCE)0733-9445(2008)134:6(890)

[10] Fang, C., Yam, M., Cheng, J., & Zhang, Y. (2015). Compressive strength and behaviour of gusset plate connections with single-sided splice members. Journal of Constructional Steel Research, 106, 166-183. doi:10.1016/j.jcsr.2014.12.009

[11] Astaneh-Asl, A. (1998). Seismic behavior and design of gusset plates. Structural Steel Educational Council.

[12] Sen, A., Roeder, C., Lehman, D., Berman, J., Sloat, D., Ballard, R., & Johnson, M. (2016). Experimental evaluation of the seismic vulnerability of braces and connections in older concentrically braced frames. Journal of Structural Engineering, 142(9). doi:10.1061/(ASCE)ST.1943-541X.0001507

[13] Tremblay, R., Filiatrault, A., Timler, P., & Bruneau, M. (1995). Performance of steel structures during the 1994 Northridge earthquake. Canadian Journal of Civil Engineering, 22(2), 338-360. doi:10.1139/l95-046

[14] Tremblay, R., Filiatrault, A., Bruneau, M., Nakashima, M., Prion, H., & DeVall, R. (1996). Seismic design of steel buildings: Lessons from the 1995 Hyogo-Ken Nanbu earthquake. Canadian Journal of Civil Engineering, 23(3), 727-756. doi:10.1139/l96-885

[15] Bradley, C., Fahnestock, L., Sizemore, J., & Hines, E. (2017). Full-scale cyclic testing of low-ductility concentrically braced frames. Journal of Structural Engineering, 143(6). doi:10.1061/(ASCE)ST.1943-541X.0001760

[16] Sizemore, J., Fahnestock, L., Hines, E., & Bradley, C. (2017). Parametric study of low-ductility concentrically braced frames under cyclic static loading. Journal of Structural Engineering, 20170601. doi:10.1061/(asce)st.1943-541x.0001761

[17] Canadian Standards Association (CSA) S16-19. (2019). Design of steel structures. Toronto, ON, Canada.

[18] Rudman, A. (2018) Testing of conventional construction W-shape brace members and their bolted end connections undergoing reversed cyclic loading. Master's thesis, Department of Civil Engineering, McGill University, Montreal, QC, Canada.

[19] Rudman, A., Tremblay, R., Rogers, C.A. (2021). Conventional I-shape brace member bolted connections under seismic loading: Laboratory study. Journal of Constructional Steel Research (Under review).

[20] Wang, C., González Ureña, A., Afifi, M., Rudman, A., Tremblay, R., Rogers, C. A. (2020) "Conventional construction steel braces with bearing plate energy dissipation", 17th World Conference on Earthquake Engineering, Sendai, Japan

[21] Wang, C., Rudman, A., Tremblay, R., Rogers, C.A. (2021). Numerical investigation into I-shape brace connections of conventional concentrically braced frames. Engineering Structures 236: 112091.

[22] Systèmes, Dassault. (2014). Abaqus 6.14 Documentation. Providence, RI: Dassault Systèmes.

[23] Yam, M., & Cheng, J. (2002). Behavior and design of gusset plate connections in compression. Journal of Constructional Steel Research, 58(5), 1143-1159. doi:10.1016/S0143-974X(01)00103-1

[24] Yam, M., Hu, S., & Cheng, J., Member, ASCE. (1994). Elastic buckling strength of gusset plate connections. Journal of Structural Engineering, 120(2), 538-559. doi:10.1061/(ASCE)0733-9445(1994)120:2(538)

[25] Goel, S., Astaneh-Asl, A., A. M. ASCE, & Hanson, R., Members, ASCE. (1985). Cyclic out-of-plane buckling of double-angle bracing. Journal of Structural Engineering, 111(5), 1135-1153. doi:10.1061/(ASCE)0733-9445(1985)111:5(1135)

[26] American Institute of Steel Construction (AISC) 341-16. (2016). Seismic provisions for structural steel buildings. Chicago, IL, USA.

[27] Walbridge, S., Grondin, G., & Cheng, J. (2005). Gusset plate connections under monotonic and cyclic loading. Canadian Journal of Civil Engineering, 32(5), 981-995. doi:10.1139/l05-045

[28] Thornton, W. A. (1984). Bracing connections for heavy construction. Engineering Journal, 21(3), 139-148.

[29] American Institute of Steel Construction (AISC) 360-16. (2016). Specification for Structural Steel Buildings. Chicago, IL, USA.